Article

Constraint on the matter–antimatter symmetry-violating phase in neutrino oscillations

https://doi.org/10.1038/s41586-020-2177-0

Received: 25 September 2019

Accepted: 3 March 2020

Published online: 15 April 2020

Check for updates

The T2K Collaboration*

The charge-conjugation and parity-reversal (CP) symmetry of fundamental particles is a symmetry between matter and antimatter. Violation of this CP symmetry was first observed in 1964[1], and CP violation in the weak interactions of quarks was soon established[2]. Sakharov proposed[3] that CP violation is necessary to explain the observed imbalance of matter and antimatter abundance in the Universe. However, CP violation in quarks is too small to support this explanation. So far, CP violation has not been observed in non-quark elementary particle systems. It has been shown that CP violation in leptons could generate the matter–antimatter disparity through a process called leptogenesis[4]. Leptonic mixing, which appears in the standard model's charged current interactions[5,6], provides a potential source of CP violation through a complex phase δ_{CP}, which is required by some theoretical models of leptogenesis[7–9]. This CP violation can be measured in muon neutrino to electron neutrino oscillations and the corresponding antineutrino oscillations, which are experimentally accessible using accelerator-produced beams as established by the Tokai-to-Kamioka (T2K) and NOvA experiments[10,11]. Until now, the value of δ_{CP} has not been substantially constrained by neutrino oscillation experiments. Here we report a measurement using long-baseline neutrino and antineutrino oscillations observed by the T2K experiment that shows a large increase in the neutrino oscillation probability, excluding values of δ_{CP} that result in a large increase in the observed antineutrino oscillation probability at three standard deviations (3σ). The 3σ confidence interval for δ_{CP}, which is cyclic and repeats every 2π, is $[-3.41, -0.03]$ for the so-called normal mass ordering and $[-2.54, -0.32]$ for the inverted mass ordering. Our results indicate CP violation in leptons and our method enables sensitive searches for matter–antimatter asymmetry in neutrino oscillations using accelerator-produced neutrino beams. Future measurements with larger datasets will test whether leptonic CP violation is larger than the CP violation in quarks.

Previous observations of neutrino oscillations have established that the three known neutrino flavour states, ν_e, ν_μ and ν_τ are mixtures of three mass states, ν_1, ν_2 and ν_3[12–15]. This mixing is described by a unitary matrix called the Pontecorvo–Maki–Nakagawa–Sakata (PMNS) matrix[16,17], which can be parameterized by three mixing angles θ_{12}, θ_{13} and θ_{23}, and complex phases. Of these phases, neutrino oscillations are sensitive to δ_{CP}. The probabilities that the neutrinos will oscillate from one flavour state to another as they travel depend on these mixing parameters and the mass squared differences ($\Delta m^2_{ij} = m^2_i - m^2_j$) between the neutrino mass states. The PMNS parameters and the mass squared differences are referred to as 'oscillation parameters'. It is known that ν_1 and ν_2 lie close to each other in mass, with $\Delta m^2_{21} = (7.53 \pm 0.18) \times 10^{-5}\ \mathrm{eV}^2/c^4$, whereas $|\Delta m^2_{32}|$ is approximately 30 times larger. However, it is not known whether m_3 has a larger or smaller mass than m_1 and m_2 (ref. [2]). The case where the mass of m_3 is larger (smaller) is called the normal (inverted) ordering. The CP symmetry-violating effect in neutrino and antineutrino oscillations has a magnitude that depends on the Jarlskog invariant[18,19]:

$$J_{CP,I} = \frac{1}{8}\cos\theta_{13}\sin(2\theta_{12})\sin(2\theta_{23})\sin(2\theta_{13})\sin\delta_{CP} \quad (1)$$

According to current measurements, this is approximately $0.033\sin\delta_{CP}$ (ref. [2]). This value has the potential to be three orders of magnitude larger than the measured quark-sector CP violation ($J_{CP,q} = 3 \times 10^{-5}$) (ref. [2]). Prior to this work, no experiment has excluded any values of δ_{CP} (taking into account both mass orderings) at the 99.73% (3σ) confidence level. T2K is a long-baseline neutrino experiment that uses beams of muon neutrinos and antineutrinos, with energy spectra peaked at

*A list of authors and their affiliations appears at the end of the paper.

0.6 GeV. We observe interactions of the neutrinos at a near detector facility 280 m from the beam production point that characterizes the beam and the interactions of the neutrinos before oscillations. The beam then propagates 295 km through the Earth to the T2K far detector, Super-Kamiokande (SK). SK measures the oscillated beam, which allows us to determine the oscillation parameters.

For this beam energy and propagation distance, the probability that muon neutrinos(antineutrinos) will oscillate to electron neutrinos (antineutrinos) is given approximately, including the CP-violating term but neglecting effects from propagation through matter, by:

$$P(\nu_\mu \to \nu_e) \approx \sin^2(2\theta_{13})\sin^2\theta_{23}\sin^2\left(\frac{1.27\Delta m^2_{32}L}{E}\right) \mp \frac{1.27\Delta m^2_{21}L}{E} 8J_{CP}\sin^2\left(\frac{1.27\Delta m^2_{32}L}{E}\right) \quad (2)$$

Here, E is the energy of the neutrino in gigaelectronvolts, the mass squared differences are given in units of eV^2/c^4, where c is the speed of light in vacuum, and L is the propagation baseline in kilometres. The second term in equation (2) has a negative sign for neutrinos and a positive sign for antineutrinos. The baseline and beam energy are optimized so that at our baseline, the probability to oscillate to electron neutrinos reaches a maximum at energies around the beam energy. Although the probability of oscillation to electron neutrinos is small, muon neutrinos also oscillate to tau neutrinos, which are not identifiable at SK because T2K's beam energy is too low for a charged tau lepton to be produced. Overall, the probability that muon neutrinos and antineutrinos will maintain their initial flavour is:

$$P(\nu_\mu \to \nu_\mu) \approx 1 - 4\cos^2\theta_{13}\sin^2\theta_{23} \times (1 - \cos^2\theta_{13}\sin^2\theta_{23})\sin^2\left(\frac{1.27\Delta m^2_{32}L}{E}\right) \quad (3)$$

Given that the probability of oscillation to tau neutrinos is large at our modal beam energy and baseline, there is a minimum in the muon neutrino energy spectrum. The position of this minimum gives the experiment sensitivity to the magnitude of Δm^2_{32} and the depth gives sensitivity to $\sin^2(2\theta_{23})$. The height of the peak in the electron neutrino energy spectrum at the oscillation maximum is, at leading order, determined by $\sin^2\theta_{23}$ and $\sin^2(2\theta_{13})$ (see equation (2)). However, it also has a sub-leading-order dependence on δ_{CP} and the neutrino mass ordering, giving sensitivity to these parameters. Owing to this interdependence, determining the other PMNS mixing parameters is important in measuring δ_{CP}. As can be seen from Fig. 1, changing δ_{CP} from $+\pi/2$ to $-\pi/2$ can lead to changes of the order of 40% in the number of electron neutrinos expected at SK. In our analysis we model the observed kinematic distributions of the final-state particles using the full oscillation probability, including the effect of the neutrinos propagating through matter, which is a perturbation of the order of 10% to the probability discussed in equations (2) and (3)[20].

The T2K neutrino beam is generated at the Japan Proton Accelerator Research Complex (J-PARC) by impinging a 30-GeV beam of protons onto a graphite target[21]. This interaction creates a large number of secondary hadrons, which are focused using magnetic horns. A neutrino (antineutrino)-enhanced beam is selected by focusing positively (negatively) charged particles—mostly pions—by choosing the polarity of the magnetic field produced by the horns, thereby enabling us to study the differences between neutrino and antineutrino oscillations. The beam axis is directed 2.5° away from the SK detector, taking advantage of the kinematics of the two-body pion decay to produce a narrow neutrino spectrum peaked at the expected energy of maximum oscillation probability[22]. The results reported here are based on SK data collected between 2009 and 2018 in neutrino (antineutrino) mode and include a beam exposure of 1.49×10^{21} (1.64×10^{21}) protons hitting the T2K neutrino production target.

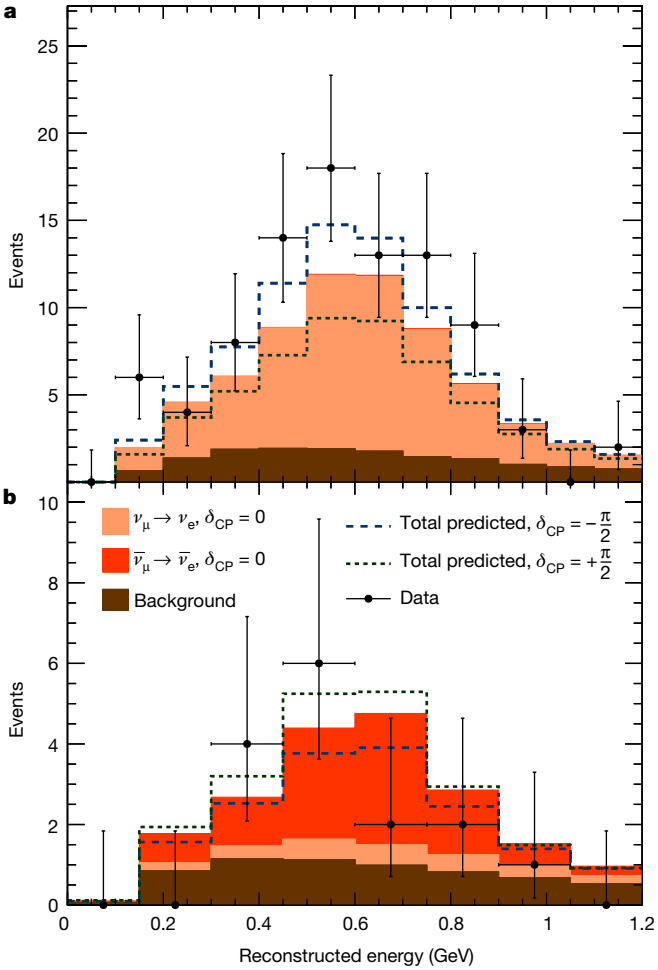

c

	1e0de ν-mode	1e0de $\bar{\nu}$-mode	1e1de ν-mode
$\nu_\mu \to \nu_e$	59.0	3.0	5.4
$\bar{\nu}_\mu \to \bar{\nu}_e$	0.4	7.5	0.0
Background	13.8	6.4	1.5
Total predicted	73.2	16.9	6.9
Systematic uncertainty	8.8%	7.1%	18.4%
Data	75	15	15

Fig. 1 | Observed ν_e and $\bar{\nu}_e$ candidate events at SK. a, **b**, The reconstructed neutrino energy spectra for the SK samples containing electron-like events in neutrino-mode (**a**) or antineutrino-mode (**b**) beam running. The uncertainty shown around the data points accounts for statistical uncertainty. The uncertainty range is chosen to include all points for which the measured number of data events is inside the 68% confidence interval of a Poisson distribution centred at that point. The solid stacked chart shows the predicted number of events for the CP-conserving point $\delta_{CP} = 0$, separated according to whether the event was from an oscillated neutrino or antineutrino or from a background process. The dashed lines show the total predicted number of events for the two most extreme CP-violating cases. **c**, The predicted number of events for $\delta_{CP} = -\pi/2$ and the measured number of events in the three electron-like samples at SK. The predicted number of events is broken down into the same categories as in **a** and **b** and the systematic uncertainty shown is after the near-detector fit. In both **a** and **b** for all predictions, normal ordering is assumed, and $\sin^2\theta_{23}$ and Δm^2_{32} are at their best-fit values. $\sin^2\theta_{13}$, $\sin^2\theta_{12}$ and Δm^2_{21} take the values indicated by external world average measurements[2]. The parameters accounting for systematic uncertainties take their best-fit values after the near-detector fit.

Neutrinos are detected by observing the particles they produce when they interact. At neutrino energies of 0.6 GeV the dominant interaction process is charged-current quasi-elastic (CCQE) scattering via the exchange of a W boson with a single neutron or proton bound in the target nucleus. In this process the neutrino (antineutrino) turns into a charged lepton (antilepton) of the same flavour. We are thereby able to identify the incoming neutrino's flavour.

Our near detector facility consists of two detectors both located 280 m downstream of the beam production target[21]. The INGRID detector[23], located on the beam axis, monitors the direction and stability of the neutrino beam. The ND280 detector[24–28] is located at the same angle away from the beam axis as SK, and characterizes the rate of neutrino interactions from the beam before oscillations have occurred, thereby reducing systematic errors. ND280 is magnetized so that charged leptons and antileptons bend in opposite directions as they traverse the detector. This effect is used to measure the fraction of events in each beam mode that are from neutrino and antineutrino interactions. In this analysis, we select samples enriched in CCQE events and also several control samples enriched in interactions from other processes, allowing their rates to be measured separately. Here we use ND280 data that include a neutrino beam exposure of 5.8×10^{20} (3.9×10^{20}) protons hitting the T2K neutrino production target in neutrino (antineutrino) mode. The explanation for the smaller dataset in ND280 and its impact on the analysis method is described in the Methods.

SK is a 50-kt water detector instrumented with photo-multiplier tube light sensors[29]. In SK, Cherenkov light is produced as charged particles above a momentum threshold travel through the water. This light is emitted in ring patterns that are detected by the light sensors. Owing to their lower mass, electrons scatter much more frequently (both elastically and inelastically) than muons, so their Cherenkov rings are blurred. We use this blurring to identify the charged lepton's flavour, as illustrated in Fig. 2. More information on the event reconstruction technique for SK data and the systematic uncertainty on SK modelling can be found in the Methods Section. SK is not magnetized, so therefore relies on ND280's measurement of the neutrino and antineutrino composition of the beam in each mode.

We form five independent samples of SK events. For both neutrino- and antineutrino-beam mode there is a sample of events that contain a single muon-like ring (denoted 1μ), and a sample of events that contain only a single electron-like ring (denoted 1e0de). These single-lepton samples are dominated by CCQE interactions. In neutrino-mode there is a sample containing an electron-like ring as well as the signature of an additional delayed electron from the decay of a charged pion and subsequent muon (denoted 1e1de). We do not use this sample in antineutrino-mode because charged pions from antineutrino interactions are mostly absorbed by a nucleus before they decay. Identifying both muon and electron neutrino interactions in both the neutrino- and antineutrino-mode beams allows us to measure the probabilities for four oscillation channels: $\nu_\mu\rightarrow\nu_\mu$ and $\bar{\nu}_\mu\rightarrow\bar{\nu}_\mu$, $\nu_\mu\rightarrow\nu_e$ and $\bar{\nu}_\mu\rightarrow\bar{\nu}_e$.

We define a model of the expected number of neutrino events as a function of kinematic variables measured in our detectors with degrees of freedom for each of the oscillation parameters and for each source of systematic uncertainty. Systematic uncertainties arise in the modelling of neutrino-nucleus interactions in the detector, the modelling of the neutrino production, and the modelling of the detector's response to neutrino interaction products. Where possible, we constrain the model using external data. For example, the solar oscillation parameters, Δm^2_{21} and $\sin^2\theta_{12}$, whose values T2K is not sensitive to, are constrained using world average data[2]. While we are sensitive to $\sin^2\theta_{13}$, we use the combination of measurements from the Daya Bay, RENO and Double Chooz reactor experiments to constrain this parameter[2], as they make a much more precise measurement than using T2K data alone (see Fig. 4a). We measure the oscillation parameters by doing a marginal likelihood fit of this model to our near and far detector data. We perform several analyses using both Bayesian and frequentist

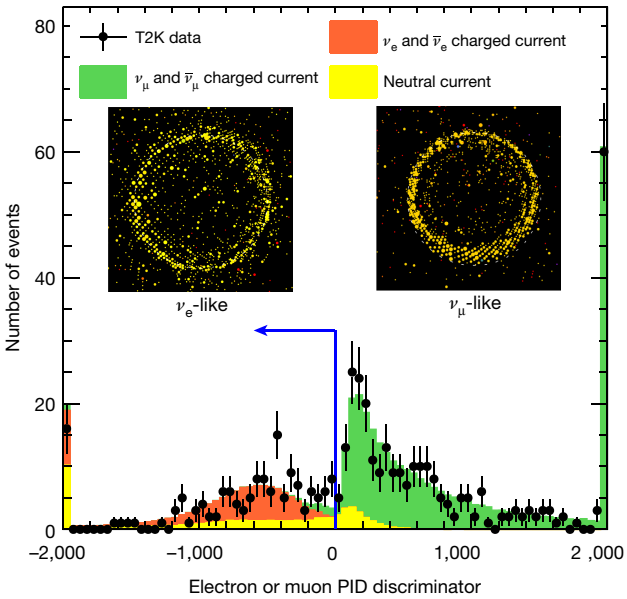

Fig. 2 | Particle identification in the SK detector. Distribution of the particle identification (PID) parameter used to classify Cherenkov rings as electron-like and muon-like. Events to the left of the blue line are classified as electron-like and those to the right as muon-like. The filled histograms show the expected number of single ring events after neutrino oscillations, with the first and last bins of the distribution containing events with discriminator values below and above the displayed range, respectively. The vertical error bars on the data points represent the standard deviations due to statistical uncertainty. The PID algorithm uses properties of the light distribution such as the blurriness of the Cherenkov ring to classify events. The insets show examples of an electron-like (left) and muon-like (right) Cherenkov ring.

statistical paradigms. Exclusive measurements of neutrino or antineutrino candidates in the near detector, one of which is shown in Fig. 3, strongly constrain the neutrino production and interaction models, reducing the uncertainty on the predicted number of events in the four single-lepton SK samples from 13–17% to 4–9%, depending on the sample. The 1e1de sample's uncertainty is reduced from 22% to 19%.

A neutrino's oscillation probability depends on its energy, as shown in equations (2) and (3). While the energy distribution of our neutrino beam is well understood, we cannot directly measure the energy of each incoming neutrino. Instead the neutrino's energy must be inferred from the momentum and direction of the charged lepton that results from the interaction. This inference relies on the correct modelling of the nuclear physics of neutrino-nucleus interactions. Modelling the strong nuclear force in multi-body problems at these energies is not computationally tractable, so approximate theories are used[30–33]. The potential biases introduced by approximations in these theories constitute the largest sources of systematic uncertainties in this measurement. For scale, the largest individual source contributes 7.1% of the overall 8.8% systematic uncertainty on the single electron-like ring ν-mode sample. Furthermore, as well as CCQE interactions, there are non-negligible contributions from interactions where additional particles were present in the final state but were not detected by our detectors. To check for bias from incorrect modelling of neutrino-nucleus interactions, we performed fits to simulated data sets generated assuming a range of different models of neutrino interactions[31,32]. We compared the measurements of the oscillation parameters obtained from these fits with the measurement from a fit to simulated data generated assuming our default model. We observed no large biases in the obtained δ_{CP} best-fit values or changes in the interval sizes from any model tested. Biases are seen on Δm^2_{32}, and these have been incorporated in the analysis through an additional

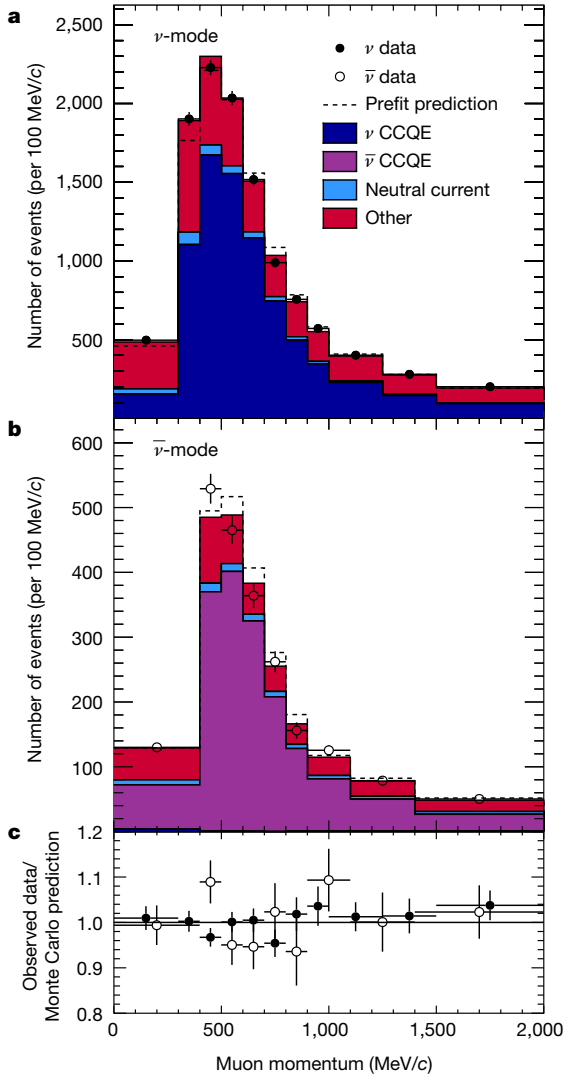

Fig. 3 | Event prediction model tuning to near-detector data. **a**, **b**, Reconstructed muon momentum in two of the ND280 CCQE-like event samples for both neutrino (**a**) and antineutrino (**b**) beam mode. The prediction with all parameters set to their best-fit value from a fit to the ND280 data are shown by the coloured histograms, split into true neutrino CCQE, antineutrino CCQE, neutral current and all other interactions. The dashed line shows the prediction before a fit to the ND280 data. The vertical error bars on the data represent the standard deviation due to statistical uncertainty. **c**, The ratio of the observed data to the best-fit Monte Carlo prediction in both neutrino-mode and antineutrino-mode samples.

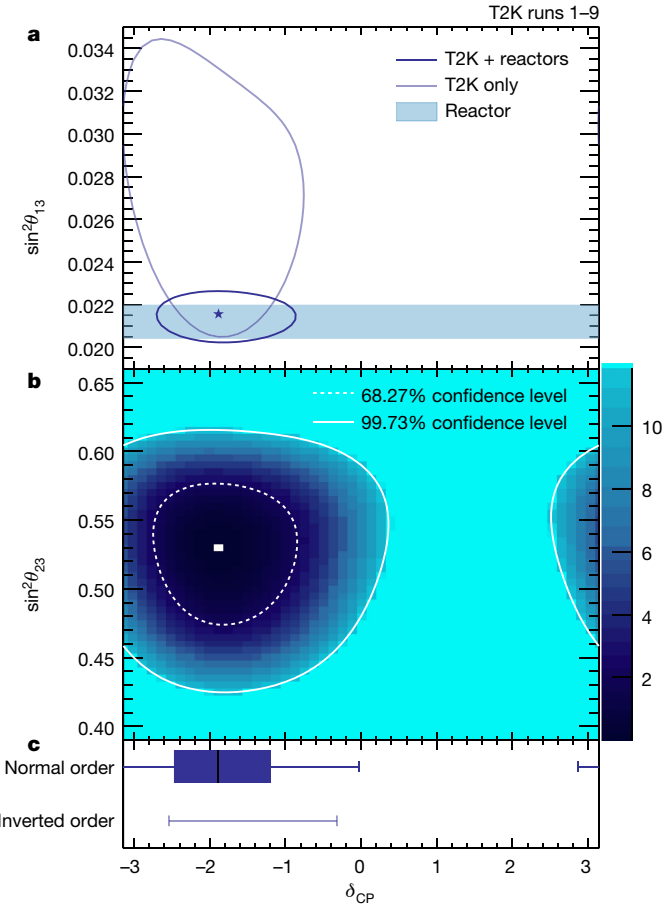

Fig. 4 | Constraints on PMNS oscillation parameters. **a**, Two-dimensional confidence intervals at the 68.27% confidence level for δ_{CP} versus $\sin^2\theta_{13}$ in the preferred normal ordering. The intervals labelled T2K only indicate the measurement obtained without using the external constraint on $\sin^2\theta_{13}$, whereas the T2K + reactor intervals do use the external constraint. The star shows the best-fit point of the T2K + reactors fit in the preferred normal mass ordering. **b**, Two-dimensional confidence intervals at the 68.27% and 99.73% confidence level for δ_{CP} versus $\sin^2\theta_{23}$ from the T2K + reactors fit in the normal ordering, with the colour scale representing the value of negative two times the logarithm of the likelihood for each parameter value. **c**, One-dimensional confidence intervals on δ_{CP} from the T2K + reactors fit in both the normal and inverted orderings. The vertical line in the shaded box shows the best-fit value of δ_{CP}, the shaded box itself shows the 68.27% confidence interval, and the error bar shows the 99.73% confidence interval. We note that there are no values in the inverted ordering inside the 68.27% interval.

error of 3.9×10^{-5} eV$^2/c^4$ on the Δm^2_{32} interval. More details of the systematic uncertainties on neutrino interaction modelling can be found in the Methods.

The observed number of events at SK can be seen in Fig. 1. The probability of observing an excess over prediction in one of our five samples at least as large as that seen in the electron-like charged pion sample is 6.9%, assuming the best-fit value of the oscillation parameters. We find that the data shows a preference for the normal mass ordering with a posterior probability of 89%, giving a Bayes factor of 8. We find $\sin^2\theta_{23} = 0.53^{+0.03}_{-0.04}$ for both mass orderings. Assuming the normal (inverted) mass ordering we find $\Delta m^2_{32} = (2.45 \pm 0.07) \times 10^{-3}$ eV$^2/c^4$ ($\Delta m^2_{13} = (2.43 \pm 0.07) \times 10^{-3}$ eV$^2/c^4$). For δ_{CP} our best-fit value and 68% (1σ) uncertainties assuming the normal (inverted) mass ordering are $-1.89^{+0.70}_{-0.58}$ ($-1.38^{+0.48}_{-0.54}$), with statistical uncertainty dominating. Our data show a preference for values of δ_{CP} that are near maximal CP violation (see Fig. 4), while both CP conserving points, $\delta_{CP} = 0$ and $\delta_{CP} = \pi$, are ruled out at the 95% confidence level. Here we also produce 99.73% (3σ) confidence and credible intervals on δ_{CP}. In the favoured normal ordering the confidence interval contains [−3.41, −0.03] (excluding 46% of the parameter space). We have investigated the effect of the excess seen in the 1e1de sample on this interval and find that had the observed number of events in this sample been as expected for the best-fit parameter values the interval would have contained [−3.71, 0.17] (excluding 38% of parameter space). In the inverted ordering the confidence interval contains [−2.54, −0.32] (excluding 65% of the parameter space). The 99.73% credible interval marginalized across both mass orderings contains [−3.48, 0.13] (excluding 42% of the parameter space). The CP-conserving points are not both excluded at the 99.73% level. However, this experiment has reported closed 99.73% (3σ) intervals on the CP-violating phase δ_{CP} (taking into account both mass orderings), and a large range of values around $+\pi/2$ are excluded.

Online content

Any methods, additional references, Nature Research reporting summaries, source data, extended data, supplementary information, acknowledgements, peer review information; details of author contributions and competing interests; and statements of data and code availability are available at https://doi.org/10.1038/s41586-020-2177-0.

1. Christenson, J. H., Cronin, J. W., Fitch, V. L. & Turlay, R. Evidence for the 2π decay of the K_2^0 meson. *Phys. Rev. Lett.* **13**, 138–140 (1964).
2. Tanabashi, M. et al. Review of particle physics. *Phys. Rev. D* **98**, 030001 (2018).
3. Sakharov, A. D. Violation of CP invariance, C asymmetry, and baryon asymmetry of the Universe. *Pis'ma Z. Eksp. Teor. Fiz.* **5**, 32–35 (1967); *Sov. Phys. Usp.* **34**, 392–393 (1991).
4. Fukugita, M. & Yanagida, T. Baryogenesis without grand unification. *Phys. Lett. B* **174**, 45–47 (1986).
5. Fukuda, Y. et al. Evidence for oscillation of atmospheric neutrinos. *Phys. Rev. Lett.* **81**, 1562–1567 (1998).
6. Ahmad, Q. R. et al. Direct evidence for neutrino flavor transformation from neutral current interactions in the Sudbury Neutrino Observatory. *Phys. Rev. Lett.* **89**, 011301 (2002).
7. Pascoli, S., Petcov, S. T. & Riotto, A. Connecting low energy leptonic CP-violation to leptogenesis. *Phys. Rev. D* **75**, 083511 (2007).
8. Hagedorn, C., Mohapatra, R. N., Molinaro, E., Nishi, C. C. & Petcov, S. T. CP violation in the lepton sector and implications for leptogenesis. *Int. J. Mod. Phys. A* **33**, 1842006 (2018).
9. Branco, G. C., González Felipe, R. & Joaquim, F. R. Leptonic *cp* violation. *Rev. Mod. Phys.* **84**, 515–565 (2012).
10. Abe, K. et al. Observation of electron neutrino appearance in a muon neutrino beam. *Phys. Rev. Lett.* **112**, 061802 (2014).
11. Acero, M. A. et al. First measurement of neutrino oscillation parameters using neutrinos and antineutrinos by NOvA. *Phys. Rev. Lett.* **123**, 151803 (2019).
12. Abe, K. et al. Search for CP violation in neutrino and antineutrino oscillations by the T2K experiment with 2.2×10^{21} protons on target. *Phys. Rev. Lett.* **121**, 171802 (2018).
13. Abe, S. et al. Precision measurement of neutrino oscillation parameters with KamLAND. *Phys. Rev. Lett.* **100**, 221803 (2008).
14. Adey, D. et al. Measurement of the electron antineutrino oscillation with 1958 days of operation at Daya Bay. *Phys. Rev. Lett.* **121**, 241805 (2018).
15. Aharmim, B. et al. Combined analysis of all three phases of solar neutrino data from the Sudbury Neutrino Observatory. *Phys. Rev. C* **88**, 025501 (2013).
16. Maki, Z., Nakagawa, M. & Sakata, S. Remarks on the unified model of elementary particles. *Prog. Theor. Phys.* **28**, 870–880 (1962).
17. Pontecorvo, B. Neutrino experiments and the problem of conservation of leptonic charge. *Sov. Phys. JETP* **26**, 984–988 (1968); *Zh. Eksp. Teor. Fiz.* **53**, 1717 (1967).
18. Krastev, P. I. & Petcov, S. T. Resonance amplification and t violation effects in three neutrino oscillations in the Earth. *Phys. Lett. B* **205**, 84–92 (1988).
19. Jarlskog, C. A basis independent formulation of the connection between quark mass matrices, CP violation and experiment. *Z. Phys. C* **29**, 491–497 (1985).
20. Barger, V., Whisnant, K., Pakvasa, S. & Phillips, R. J. N. Matter effects on three-neutrino oscillations. *Phys. Rev. D* **22**, 2718–2726 (1980).
21. Abe, K. et al. The T2K experiment. *Nucl. Instrum. Methods A* **659**, 106–135 (2011).
22. Beavis, D., Carroll, A., Chiang, I. & the E889 Collaboration. *Long Baseline Neutrino Oscillation Experiment At The AGS* Physics design report BNL No. 52459 https://doi.org/10.2172/52878 (Brookhaven National Laboratory, 1995).
23. Otani, M. et al. Design and construction of INGRID neutrino beam monitor for T2K neutrino experiment. *Nucl. Instrum. Methods A* **623**, 368–370 (2010).
24. Amaudruz, P. A. et al. The T2K fine-grained detectors. *Nucl. Instrum. Methods A* **696**, 1–31 (2012).
25. Assylbekov, S. et al. The T2K ND280 off-axis pi-zero detector. *Nucl. Instrum. Methods A* **686**, 48–63 (2012).
26. Abgrall, N. et al. Time projection chambers for the T2K near detectors. *Nucl. Instrum. Methods A* **637**, 25–46 (2011).
27. Allan, D. et al. The electromagnetic calorimeter for the T2K near detector ND280. *J. Instrum.* **8**, P10019 (2013).
28. Aoki, S. et al. The T2K Side Muon Range Detector (SMRD). *Nucl. Instrum. Methods A* **698**, 135–146 (2013).
29. Fukuda, Y. et al. The Super-Kamiokande detector. *Nucl. Instrum. Methods A* **501**, 418–462 (2003).
30. Nieves, J., Valverde, M. & Vicente Vacas, M. J. Inclusive nucleon emission induced by quasi-elastic neutrino-nucleus interactions. *Phys. Rev. C* **73**, 025504 (2006).
31. Martini, M., Ericson, M., Chanfray, G. & Marteau, J. A unified approach for nucleon knock-out, coherent and incoherent pion production in neutrino interactions with nuclei. *Phys. Rev. C* **80**, 065501 (2009).
32. Benhar, O., Farina, N., Nakamura, H., Sakuda, M. & Seki, R. Electron- and neutrino-nucleus scattering in the impulse approximation regime. *Phys. Rev. D* **72**, 053005 (2005).
33. Salcedo, L. L., Oset, E., Vicente-Vacas, M. J. & Garcia-Recio, C. Computer simulation of inclusive pion nuclear reactions. *Nucl. Phys. A* **484**, 557–592 (1988).

Publisher's note Springer Nature remains neutral with regard to jurisdictional claims in published maps and institutional affiliations.

© The Author(s), under exclusive licence to Springer Nature Limited 2020

The T2K Collaboration

K. Abe[1], R. Akutsu[2], A. Ali[3], C. Alt[4], C. Andreopoulos[5,6], L. Anthony[6], M. Antonova[7], S. Aoki[8], A. Ariga[9], T. Arihara[10], Y. Asada[11], Y. Ashida[3], E. T. Atkin[12], Y. Awataguchi[10], S. Ban[3], M. Barbi[13], G. J. Barker[14], G. Barr[15], D. Barrow[15], C. Barry[6], M. Batkiewicz-Kwasniak[16], A. Beloshapkin[17], F. Bench[6], V. Berardi[18], S. Berkman[19,20], L. Berns[21], S. Bhadra[22], S. Bienstock[23], A. Blondel[23,24], S. Bolognesi[25], B. Bourguille[26], S. B. Boyd[14], D. Brailsford[27], A. Bravar[24], D. Bravo Berguño[28], C. Bronner[1], A. Bubak[29], M. Buizza Avanzini[30], J. Calcutt[31], T. Campbell[32], S. Cao[33], S. L. Cartwright[34], M. G. Catanesi[18], A. Cervera[7], A. Chappell[14], C. Checchia[35], D. Cherdack[36], N. Chikuma[37], M. Cicerchia[35], G. Christodoulou[38], J. Coleman[6], G. Collazuol[35], L. Cook[15,39], D. Coplowe[15], A. Cudd[31], A. Dabrowska[16], G. De Rosa[40], T. Dealtry[27], P. F. Denner[14], S. R. Dennis[6], C. Densham[5], F. Di Lodovico[41], N. Dokania[42], S. Dolan[38], T. A. Doyle[27], O. Drapier[30], J. Dumarchez[23], P. Dunne[12], A. Eguchi[37], L. Eklund[43], S. Emery-Schrenk[25], A. Ereditato[9], P. Fernandez[7], T. Feusels[19,20], A. J. Finch[27], G. A. Fiorentini[22], G. Fiorillo[40], C. Francois[9], M. Friend[33], Y. Fujii[33], R. Fujita[37], D. Fukuda[44], R. Fukuda[45], Y. Fukuda[46], K. Fusshoeller[4], K. Gameil[19,20], C. Giganti[23], T. Golan[47], M. Gonin[30], A. Gorin[17], M. Guigue[23], D. R. Hadley[14], J. T. Haigh[14], P. Hamacher-Baumann[48], M. Hartz[20,39]✉, T. Hasegawa[33], S. Hassani[25], N. C. Hastings[33], T. Hayashino[3], Y. Hayato[1,39], A. Hiramoto[3], M. Hogan[49], J. Holeczek[29], N. T. Hong Van[50,51], F. Iacob[35], A. K. Ichikawa[3], M. Ikeda[1], T. Ishida[33], T. Ishii[33], M. Ishitsuka[45], K. Iwamoto[37], A. Izmaylov[7,17], M. Jakkapu[33], B. Jamieson[52], S. J. Jenkins[34], C. Jesús-Valls[26], M. Jiang[3], S. Johnson[32], P. Jonsson[12], C. K. Jung[42], X. Junjie[2], P. B. Jurj[12], M. Kabirnezhad[15], A. C. Kaboth[5,53], T. Kajita[2,39], H. Kakuno[10], J. Kameda[1], D. Karlen[20,54], S. P. Kasetti[55], Y. Kataoka[1], T. Katori[41], Y. Kato[1], E. Kearns[39,56], M. Khabibullin[17], A. Khotjantsev[17], T. Kikawa[3], H. Kikutani[37], H. Kim[57], J. Kim[19,20], S. King[41], J. Kisiel[29], A. Knight[14], A. Knox[27], T. Kobayashi[33], L. Koch[15], T. Koga[37], A. Konaka[20], L. L. Kormos[27], Y. Koshio[39,44], A. Kostin[17], K. Kowalik[58], H. Kubo[3], Y. Kudenko[17,59], N. Kukita[57], S. Kuribayashi[3], R. Kurjata[60], T. Kutter[55], M. Kuze[21], L. Labarga[28], J. Lagoda[58], M. Lamoureux[35], M. Laveder[35], M. Lawe[27], M. Licciardi[30], T. Lindner[20], R. P. Litchfield[43], S. L. Liu[42], X. Li[42], A. Longhin[35], L. Ludovici[61], X. Lu[15], T. Lux[26], L. N. Machado[40], L. Magaletti[18], K. Mahn[31], M. Malek[34], S. Manly[62], L. Maret[24], A. D. Marino[32], L. Marti-Magro[1,39], J. F. Martin[63], T. Maruyama[33], T. Matsubara[33], K. Matsushita[37], V. Matveev[17], K. Mavrokoridis[6], E. Mazzucato[25], M. McCarthy[22], N. McCauley[6], J. McElwee[34], K. S. McFarland[62], C. McGrew[42], A. Mefodiev[17], C. Metelko[6], M. Mezzetto[35], A. Minamino[11], O. Mineev[17], S. Mine[64], M. Miura[1,39], L. Molina Bueno[4], S. Moriyama[1,39], J. Morrison[31], Th. A. Mueller[30], L. Munteanu[25], S. Murphy[4], Y. Nagai[32], T. Nakadaira[33], M. Nakahata[1,39], Y. Nakajima[1], A. Nakamura[44], K. G. Nakamura[3], K. Nakamura[33,39], S. Nakayama[1,39], T. Nakaya[3,39], K. Nakayoshi[33], C. Nantais[63], C. E. R. Naseby[12], T. V. Ngoc[50], K. Niewczas[47], K. Nishikawa[33,71], Y. Nishimura[65], E. Noah[24], T. S. Nonnenmacher[12], F. Nova[5], P. Novella[7], J. Nowak[27], J. C. Nugent[43], H. M. O'Keeffe[27], L. O'Sullivan[34], T. Odagawa[3], K. Okumura[2,39], T. Okusawa[57], S. M. Oser[19,20], R. A. Owen[66], Y. Oyama[33], V. Palladino[40], J. L. Palomino[42], V. Paolone[67], M. Pari[35], W. C. Parker[53], S. Parsa[24], J. Pasternak[12], P. Paudyal[6], M. Pavin[20], D. Payne[6], G. C. Penn[6], L. Pickering[31], C. Pidcott[34], G. Pintaudi[11], E. S. Pinzon Guerra[22], C. Pistillo[9], B. Popov[23], K. Porwit[29], M. Posiadala-Zezula[68], A. Pritchard[6], B. Quilain[39], T. Radermacher[48], E. Radicioni[18], B. Radics[4], P. N. Ratoff[27], E. Reinherz-Aronis[49], C. Riccio[40], E. Rondio[58], S. Roth[48], A. Rubbia[4], A. C. Ruggeri[40], C. A. Ruggles[43], A. Rychter[60], K. Sakashita[33], F. Sánchez[24], G. Santucci[22], C. M. Schloesser[4], K. Scholberg[39,69], J. Schwehr[49], M. Scott[12], Y. Seiya[57], T. Sekiguchi[33], H. Sekiya[1,39], D. Sgalaberna[38], R. Shah[5,15], A. Shaikhiev[17], F. Shaker[52], A. Shaykina[17], M. Shiozawa[1,39], W. Shorrock[12], A. Shvartsman[17], A. Smirnov[17], M. Smy[64], J. T. Sobczyk[47], H. Sobel[39,64], F. J. P. Soler[43], Y. Sonoda[1], J. Steinmann[48], S. Suvorov[17,25], A. Suzuki[8], S. Y. Suzuki[33], Y. Suzuki[39], A. A. Sztuc[12], M. Tada[33], M. Tajima[3], A. Takeda[1], Y. Takeuchi[8,39], H. K. Tanaka[1,39], H. A. Tanaka[63,70], S. Tanaka[57], L. F. Thompson[34], W. Toki[49], C. Touramanis[6], T. Towstego[63], K. M. Tsui[6], T. Tsukamoto[33], M. Tzanov[55], Y. Uchida[12], W. Uno[3], M. Vagins[39,64], S. Valder[14], Z. Vallari[42], D. Vargas[26], G. Vasseur[25], C. Vilela[42], W. G. S. Vinning[14], T. Vladisavljevic[15,39], V. V. Volkov[17], T. Wachala[16], J. Walker[52], J. G. Walsh[27], Y. Wang[42], D. Wark[5,15], M. O. Wascko[12], A. Weber[5,15], R. Wendell[3,39], M. J. Wilking[42], C. Wilkinson[9], J. R. Wilson[41], R. J. Wilson[49], K. Wood[42], C. Wret[62], Y. Yamada[33,71], K. Yamamoto[57], C. Yanagisawa[42], G. Yang[42], T. Yano[1], K. Yasutome[3], S. Yen[20], N. Yershov[17], M. Yokoyama[37,39], T. Yoshida[21], M. Yu[22], A. Zalewska[16], J. Zalipska[58], K. Zaremba[60], G. Zarnecki[58], M. Ziembicki[60], E. D. Zimmerman[32], M. Zito[23], S. Zsoldos[41] & A. Zykova[17]

[1]Institute for Cosmic Ray Research, Kamioka Observatory, University of Tokyo, Kamioka, Japan. [2]Institute for Cosmic Ray Research, Research Center for Cosmic Neutrinos, University of Tokyo, Kashiwa, Japan. [3]Department of Physics, Kyoto University, Kyoto, Japan. [4]Institute for Particle Physics and Astrophysics, ETH Zurich, Zurich, Switzerland. [5]STFC, Rutherford Appleton Laboratory, Didcot, UK. [6]Department of Physics, University of Liverpool, Liverpool, UK. [7]IFIC (CSIC and University of Valencia), Valencia, Spain. [8]Kobe University, Kobe, Japan. [9]Albert Einstein Center for Fundamental Physics, Laboratory for High Energy Physics (LHEP), University of Bern, Bern, Switzerland. [10]Department of Physics, Tokyo Metropolitan University, Tokyo, Japan. [11]Faculty of Engineering, Yokohama National University, Yokohama, Japan. [12]Department of Physics, Imperial College London, London, UK. [13]Department of Physics, University of Regina, Regina, Saskatchewan, Canada. [14]Department of Physics, University of Warwick, Coventry, UK. [15]Department of Physics, Oxford University, Oxford, UK. [16]H. Niewodniczanski Institute of Nuclear Physics PAN, Cracow, Poland. [17]Institute for Nuclear Research of the Russian Academy of Sciences, Moscow, Russia. [18]Dipartimento Interuniversitario di Fisica, INFN Sezione di Bari and Università e Politecnico di Bari, Bari, Italy. [19]Department of Physics and Astronomy, University of British Columbia, Vancouver, British Columbia, Canada. [20]TRIUMF, Vancouver, British Columbia, Canada. [21]Department of Physics, Tokyo Institute of Technology, Tokyo, Japan. [22]Department of Physics and Astronomy, York

University, Toronto, Ontario, Canada. [23]Laboratoire de Physique Nucléaire et de Hautes Energies (LPNHE), Sorbonne Université, Université Paris Diderot, CNRS/IN2P3, Paris, France. [24]Section de Physique, DPNC, University of Geneva, Geneva, Switzerland. [25]IRFU, CEA Saclay, Gif-sur-Yvette, France. [26]Institut de Fisica d'Altes Energies (IFAE), The Barcelona Institute of Science and Technology, Barcelona, Spain. [27]Physics Department, Lancaster University, Lancaster, UK. [28]Department of Theoretical Physics, University Autonoma Madrid, Madrid, Spain. [29]Institute of Physics, University of Silesia, Katowice, Poland. [30]Ecole Polytechnique, IN2P3-CNRS, Laboratoire Leprince-Ringuet, Palaiseau, France. [31]Department of Physics and Astronomy, Michigan State University, East Lansing, MI, USA. [32]Department of Physics, University of Colorado at Boulder, Boulder, CO, USA. [33]High Energy Accelerator Research Organization (KEK), Tsukuba, Japan. [34]Department of Physics and Astronomy, University of Sheffield, Sheffield, UK. [35]Dipartimento di Fisica e Astronomia, INFN Sezione di Padova and Università di Padova, Padua, Italy. [36]Department of Physics, University of Houston, Houston, TX, USA. [37]Department of Physics, University of Tokyo, Tokyo, Japan. [38]CERN European Organization for Nuclear Research, Geneva, Switzerland. [39]Kavli Institute for the Physics and Mathematics of the Universe (WPI), The University of Tokyo Institutes for Advanced Study, University of Tokyo, Chiba, Japan. [40]Dipartimento di Fisica, INFN Sezione di Napoli and Università di Napoli, Naples, Italy. [41]Department of Physics, King's College London, London, UK. [42]Department of Physics and Astronomy, State University of New York at Stony Brook, Stony Brook, NY, USA. [43]School of Physics and Astronomy, University of Glasgow, Glasgow, UK. [44]Department of Physics, Okayama University, Okayama, Japan. [45]Department of Physics, Faculty of Science and Technology, Tokyo University of Science, Chiba, Japan. [46]Department of Physics, Miyagi University of Education, Sendai, Japan. [47]Faculty of Physics and Astronomy, Wroclaw University, Wroclaw, Poland. [48]III. Physikalisches Institut, RWTH Aachen University, Aachen, Germany. [49]Department of Physics, Colorado State University, Fort Collins, CO, USA. [50]Institute For Interdisciplinary Research in Science and Education (IFIRSE), ICISE, Quy Nhon, Vietnam. [51]International Centre of Physics, Institute of Physics (IOP), Vietnam Academy of Science and Technology (VAST), Hanoi, Vietnam. [52]Department of Physics, University of Winnipeg, Winnipeg, Manitoba, Canada. [53]Department of Physics, Royal Holloway University of London, Egham, UK. [54]Department of Physics and Astronomy, University of Victoria, Victoria, British Columbia, Canada. [55]Department of Physics and Astronomy, Louisiana State University, Baton Rouge, LA, USA. [56]Department of Physics, Boston University, Boston, MA, USA. [57]Department of Physics, Osaka City University, Osaka, Japan. [58]National Centre for Nuclear Research, Warsaw, Poland. [59]National Research Nuclear University "MEPhI", Moscow Institute of Physics and Technology, Moscow, Russia. [60]Institute of Radioelectronics and Multimedia Technology, Warsaw University of Technology, Warsaw, Poland. [61]INFN Sezione di Roma and Università di Roma "La Sapienza", Rome, Italy. [62]Department of Physics and Astronomy, University of Rochester, Rochester, NY, USA. [63]Department of Physics, University of Toronto,, Toronto, Ontario, Canada. [64]University of California, Irvine, Department of Physics and Astronomy, Irvine, CA, USA. [65]Department of Physics, Keio University, Kanagawa, Japan. [66]School of Physics and Astronomy, Queen Mary University of London, London, UK. [67]Department of Physics and Astronomy, University of Pittsburgh, Pittsburgh, PA, USA. [68]Faculty of Physics, University of Warsaw, Warsaw, Poland. [69]Department of Physics, Duke University, Durham, NC, USA. [70]SLAC National Accelerator Laboratory, Stanford University, Menlo Park, CA, USA. [71]Deceased: Y. Yamada, K. Nishikawa. ✉e-mail: mhartz@triumf.ca

Methods

The measurement presented in this paper relies on the modelling of experimental apparatus to infer the parameters governing the oscillations of neutrinos. This modelling can be broken into three main categories: the modelling of the neutrino production in the beamline, the modelling of neutrino–nucleus interactions in the detectors, and the modelling of the detectors' responses to final-state particles and the inference of particle properties from the detector response. The main sources of systematic uncertainty in the data analysis arise in these three areas, and here we provide a description of the models and associated systematic uncertainties.

The inference of neutrino oscillation parameters from the data also relies on the statistical methods applied. In this section, we also provide a detailed description of the statistical methods used to infer the favoured values and allowed regions for neutrino oscillation parameters.

Neutrino production modelling

The predicted neutrino and antineutrino fluxes, including the energies and flavours of neutrinos and antineutrinos, are estimated using a detailed simulation of the T2K beamline. Measurement of the proton beam orbit, transverse width and divergence, and intensity are used as the initial conditions before simulating the interactions of protons in the T2K target to produce the secondary particles that decay to neutrinos. Particle interactions and production inside the target are simulated with FLUKA2011[34,35], while particle propagation outside the target is simulated with GEANT3[36]. Interaction rates and hadron production in the simulation are tuned with hadron interaction data from external experiments, primarily the NA61/SHINE experiment, which has collected data for T2K at the J-PARC proton beam energy of 30 GeV with the T2K target material of graphite[37]. Measurements of the currents of the magnetic horns during beam operation and of the magnetic fields of the horns before installation ensure accurate modelling of the charged particle focusing in the flux simulation. The simulated fluxes are used as inputs to simulations of neutrino interactions and particle detection in the ND280 and SK detectors. The spectrum of muon neutrinos or antineutrinos produced from the decays of focused charged pions peaks at an energy of 0.6 GeV for an off-axis angle of 2.5°. Near the peak energy, 97.2% (96.2%) of the neutrino-mode (antineutrino-mode) beam is initially ν_μ ($\bar{\nu}_\mu$). The remaining components are mostly $\bar{\nu}_\mu$ (ν_μ); contaminations of $\nu_e + \bar{\nu}_e$ are only 0.47% (0.49%).

Since the neutrino flux prediction depends on the measured beam and beamline properties, which may vary with time, different flux predictions are made for each run period, and they are combined with weights proportional to the number of protons-on-target (POT) accumulated during periods of nominal detector operation. The collected ND280 data corresponds to 5.8×10^{20} POT in neutrino mode and 3.9×10^{20} POT in antineutrino mode. This amount is less than the amount of data collected at SK owing to the lower efficiency of nominal data taking at ND280, and longer data processing times for ND280 data, limiting the available dataset. This POT difference between ND280 and SK is accounted for by combining the POT-weighted flux predictions for each run period based on the beam exposures for the data collected at each detector.

The uncertainty on the flux calculation is evaluated by propagating uncertainties on the proton beam measurements, hadronic interactions, material modelling and alignment of beamline elements, and horn current and field measurements. In each case, variations of the source of uncertainty are considered and the effect on the flux simulation is evaluated. The INGRID on-axis neutrino detector is not used to tune the beam direction during operation. Hence, it provides an independent measurement of the beam direction[38], which is used to validate the flux simulation. The uncertainty on the INGRID beam direction measurement is propagated in the flux model. The variations are used to calculate covariances for the flux prediction in bins of energy, flavour, neutrino/antineutrino mode and detector (ND280 and SK). These covariances are used to propagate uncertainties on the flux prediction in the oscillation analysis. The dominant source of systematic uncertainty is from the hadron interaction data and models. The uncertainty on the flux normalization in this analysis near the peak energy of 0.6 GeV is 9%. In future analyses we aim to improve this to approximately 5% by using NA61/SHINE particle production data measured from a replica of the T2K target[39,40]. Uncertainties on the proton beam orbit and alignment of beamline elements correspond to an uncertainty on the off-axis angle at the ND280 and SK detectors, corresponding to uncertainties on the peak energy of the neutrino spectrum at those detectors.

Neutrino interaction modelling

The T2K detectors measure products of neutrinos and antineutrinos interacting on nuclei and free protons with energies ranging from about 0.1 GeV to 30 GeV. These interactions are modelled with the NEUT[41] neutrino interaction generator, using version 5.3.2. NEUT uses a range of models to describe the physics of the initial nuclear state, the neutrino–nucleon(s) interaction, and the interactions of final-state particles in the nuclear medium.

The primary signal processes in SK are defined by the presence of a single charged lepton candidate with no other visible particles. The dominant process at the peak energy of 0.6 GeV is CCQE scattering. This process corresponds to the neutrino or antineutrino scattering on a single nucleon bound in the target nucleus. The neutrino–nucleon scattering in NEUT is implemented in the formalism of Llewellyn–Smith[42]. For the initial nuclear state, NEUT implements a relativistic Fermi gas model of the target nucleus, including long-range correlations evaluated using the random phase approximation[43]. NEUT includes an alternative initial-state model based on spectral functions describing the initial momentum and removal energy for bound nucleons[44].

Additional processes that can produce a signal-like final state are modelled in NEUT. The two-particle, two-hole (2p-2h) model of Nieves et al.[45,46] predicts the production of multinucleon excitations, where more than one nucleon and no pions are ejected in the final state. The ejected nucleons are typically below the detection threshold in a water Cherenkov detector, making this process indistinguishable from the CCQE process.

The signal candidate sample with one prompt electron-like ring and the presence of an electron from muon decay consists primarily of interactions where a pion is produced. These single-pion interactions can also populate the samples without an additional electron from muon decay if the pion is absorbed in the target nucleus or on a nucleus in the detector, or if it is not detected. Processes producing a single pion and one nucleon are described by the Rein–Sehgal model[47]. Processes with multiple pions are simulated with a custom model below 2 GeV of hadronic invariant mass and by PYTHIA[48] otherwise. These processes may be selected as events with single Cherenkov rings if the pion is absorbed in the target nucleus or surrounding nuclei, or if it is not detected. The final-state interactions of pions and protons in the target nucleus are modelled with the NEUT intranuclear cascade model where the density dependence of the mean free path for pions in the target nucleus is calculated based on the Δ-hole model of ref. [49] at low momenta and from $p-\pi$ scattering data from the SAID database at high momenta. The microscopic interaction rates for exclusive pion scattering modes are then tuned to macroscopic π–nucleus scattering data.

We consider two types of systematic uncertainties on neutrino interaction modelling in the oscillation measurement. In the first, parameters in the nominal interaction model are allowed to vary and are constrained by ND280 data. These parameters are then marginalized over when measuring oscillation parameters. They include uncertainties on nucleon form factors, the corrections for long-range correlations, the rates of different neutrino interaction processes, the final-state kinematics of the CCQE, 2p-2h and single-pion production

processes, and the rates of pion final-state interactions. Most of these are parameters in the models with physical interpretations, and they modify the overall rate of interactions, the final-state topology, and the kinematics of final-state particles. After the constraint from ND280 data, these parameters are correlated with the systematic parameters in the neutrino production model, and their combined impact on the predicted event distributions in SK is evaluated. The constrained interaction model and neutrino production model parameters contribute a 2.7% uncertainty on the prediction of the relative number of electron neutrino and electron antineutrino candidates, the third-largest source of systematic uncertainty, as shown in Extended Data Table 1.

We also include an uncertainty on the ν_e and $\bar{\nu}_e$ cross-sections relative to the ν_μ and $\bar{\nu}_\mu$ cross-sections. This introduces a direct uncertainty on the relative prediction of ν_e and $\bar{\nu}_e$ candidates, and is motivated by uncertainties in the neutrino–nucleon scattering cross-section arising from the charged lepton masses[50]. As shown in Extended Data Table 1, this introduces a relative uncertainty of 3.0%, the second-largest single source of systematic uncertainty in the CP asymmetry measurement.

The second type of systematic uncertainty is evaluated by introducing simulated data generated by an alternative model into the analysis and evaluating the impact on measured oscillation parameters. This approach is used to evaluate the effect of changing the nuclear initial-state model including the use of the spectral functions and changes to the removal energy for initial-state nucleons. This approach is also applied to evaluate the impact of changes to the 2p-2h interaction cross-section as a function of energy, using an alternative single-pion production model[51,52], and applying alternative multi-pion production tuning[53]. The largest biases observed in this approach are on the measurement of Δm^2_{32}, whereas the impact on other parameters is typically small compared to the total systematic uncertainty. In the case of Δm^2_{32}, an additional uncertainty of $3.9\times10^{-5}\,\mathrm{eV}^2/c^4$ is included by taking a convolution of a Gaussian of width $3.9\times10^{-5}\,\mathrm{eV}^2/c^4$ with the likelihood. For the measurement of the other oscillation parameters, we found that the biases introduced by varying the removal energy by up to 18 MeV for initial-state nucleons were not negligible. An additional uncertainty equal to the bias in the predicted event distributions when varying the removal energy by 18 MeV was therefore added to the analysis. As shown in Extended Data Table 1, this introduces a 3.7% uncertainty on the relative prediction of electron neutrino and electron antineutrino candidates, the largest single source of systematic uncertainty in the analysis.

SK event reconstruction

Photosensors installed on the SK inner detector register Cherenkov light, produced as charged particles produced by neutrino interactions travel through the water volume[29]. Photosensor activity clustered in time, on the order of a microsecond, is termed an event. Events coincident with the T2K-beam timing are selected as candidate beam neutrino interactions.

Neutrino interaction events in SK often have multiple periods of photosensor activity separated in time within an event. The most frequent example is a muon decaying into an electron. A decay electron can be used to tag a muon even when the muon energy is below the Cherenkov threshold, for example, the case that the muon is produced by a charged pion decaying at rest. Such sub-events are searched for with a peak finding algorithm and reconstructed separately in later processes.

The kinematics of the charged particles are reconstructed from the timing and the number of detected photons of each photosensor signal by using a maximum likelihood algorithm[54]. The likelihood consists of the probability of each photosensor to detect photons or not and the charge and timing probability density functions of the hit photosensors. This new reconstruction algorithm makes use of the timing and charge information obtained by all the photosensors simultaneously, which leads to better kinematic resolutions and particle-classifying performances compared to the previously used reconstruction algorithm.

The five signal samples are formed by using the reconstructed event kinematics. All the selected events are required to have little photosensor activity in an outer veto detector, and the reconstructed neutrino interaction position is required to be inside the inner detector fiducial volume. The reconstruction improvement enabled us to extend the fiducial volumes used in the analysis. We performed a dedicated study to optimize the fiducial volume to maximize T2K sensitivities to oscillation parameters taking into account both the statistical and systematical uncertainties. The position-dependent SK detector systematics are estimated by using SK atmospheric neutrino interaction events. The fiducial volume expansion contributes to the increase of selected electron-like (muon-like) events by 25% (14%)[12].

Systematic uncertainties regarding SK detector modelling were addressed by various control samples. Uncertainties on the position reconstruction bias and on the decay electron tagging are estimated by using cosmic-ray muons stopping inside the inner detector. Simulated atmospheric neutrino events are compared to data to evaluate systematic uncertainties on the modelling of signal selection efficiencies and the background contamination of the five analysis samples. Parameters describing possible mis-modelling of Cherenkov ring counting and particle identifications are introduced and constrained by a fit to the control samples. These parameters are varied according to the posterior distribution from the fit to the control samples, and the uncertainties on the T2K samples of interest are evaluated. The uncertainty on the modelling of the efficiency of selecting events with neutral pions, which is one of the dominant backgrounds in the electron neutrino CCQE-like event sample, is estimated by constructing a set of hybrid events that combine one data-derived electron-like Cherenkov ring and one simulated electron-like Cherenkov ring to imitate the decay of a neutral pion. The uncertainties on the numbers of selected total events in SK are 2–4% depending on the signal categories. As shown in Extended Data Table 1, the relative uncertainty on the predicted number of electron neutrino and electron antineutrino candidates for samples with no decay electrons is 1.5%.

Statistical methods

We use a binned likelihood-ratio method comparing the observed and predicted numbers of muon-neutrino and electron-neutrino candidate events in our five samples. In neutrino beam mode these are electron-like, muon-like and electron-like charged pion samples, whereas in antineutrino beam mode these are electron-like and muon-like samples. The samples are binned in reconstructed energy and, for the electron-neutrino-like samples, the angle between the lepton and the beam direction. In particular, best-fits are determined by minimizing the sum of the following likelihood function (marginalized over nuisance parameters) over all of our samples:

$$-2\ln\lambda(\overline{\delta_{\mathrm{CP}}};\mathbf{a}) = 2\sum_{i=1}^{N}\left[n_i^{\mathrm{obs}}\ln\left(\frac{n_i^{\mathrm{obs}}}{n_i^{\mathrm{exp}}}\right)+n_i^{\mathrm{exp}}-n_i^{\mathrm{obs}}\right] + (\mathbf{a}-\mathbf{a}_0)^{\mathrm{T}}\mathbf{C}^{-1}(\mathbf{a}-\mathbf{a}_0) \quad (4)$$

where $\overline{\delta_{\mathrm{CP}}}$ is the estimated value of δ_{CP}, $\mathbf{a}$ is the vector of systematic parameter values (including the remaining oscillation parameters), $\mathbf{a}_0$ is the vector of default values of the systematic parameters, $\mathbf{C}$ is the systematic parameter covariance matrix, N is the number of reconstructed energy and lepton angle bins, n_i^{obs} is the number of events observed in bin i and $n_i^{\mathrm{exp}} = n_i^{\mathrm{exp}}(\overline{\delta_{\mathrm{CP}}};\mathbf{a})$ is the corresponding expected number of events. Systematic parameters are marginalized according to their prior constraints from the fit to ND280 data.

We perform both frequentist and Bayesian analyses of our data. The measurement of δ_{CP} from each of the analyses is in agreement, with the presented confidence intervals coming from a frequentist analysis and the Bayes factors and credible intervals coming from a Bayesian analysis. In the frequentist analysis a fit is first performed to the near

detector samples binned in the momentum and cosine of the angle between the lepton and the beam direction, with penalty terms for flux, cross-section and detector systematic parameters at the near detector. Systematic parameter constraints are then propagated from the near to the far detector via the covariance matrix, **C**, in equation (4) and their fitted values. The matrix is the combination of the posterior covariance from the near detector fit with the priors for the oscillation parameters, with some parameters affecting both detectors directly, whereas others that affect only the far detector are constrained through their correlation with near-detector-affecting parameters. Gaussian priors for $\sin^2\theta_{13}$, $\sin^2\theta_{12}$, and Δm^2_{21} are taken from the Particle Data Group's world combinations[2], while $\sin^2\theta_{23}$ and Δm^2_{32} (Δm^2_{13}) have uniform priors in normal (inverted) mass ordering. For the Bayesian analyses the prior for δ_{CP} is uniform, with an additional check applying a uniform prior in $\sin\delta_{CP}$ producing the same conclusions. Furthermore, rather than fitting the near detector and propagating to the far detector as a two-step process, the Bayesian analysis directly includes the near detector samples in its expression for the likelihood and therefore performs a simultaneous fit of the near and far detector data.

The neutrino oscillation probability depends nonlinearly on the oscillation parameters, with different possible values of δ_{CP} corresponding to a bounded enhancement or suppression of the electron (anti) neutrino appearance probability. If statistical fluctuations in the data exceed these bounds, they are not accommodated by the model, and as a result the critical $\Delta\chi^2$ value for a given confidence level is often different from the asymptotic rule of Wilks[55]. To address this problem the frequentist analysis constructs Neyman confidence intervals using the approach described by Feldman and Cousins[56] and thus critical values of $\Delta\chi^2$ vary as a function of δ_{CP} and the mass ordering. The critical values at a given confidence level are determined by fitting at least 20,000 simulated datasets for each given true value of δ_{CP} and the mass ordering. The remaining oscillation parameters are varied according to their priors. In particular, for $\sin^2\theta_{13}$, $\sin^2\theta_{12}$ and Δm^2_{21} these priors are taken from the Particle Data Group[2], with $\sin^2\theta_{13}$ determined by the reactor experiments noted in the main text. For $\sin^2\theta_{23}$, and Δm^2_{32} (Δm^2_{13}) the priors take the form of likelihood surfaces produced from fits of simulated datasets. The simulated datasets are generated using oscillation parameter best-fits in normal and inverted mass orderings. The remaining systematic parameters are varied according to their prior constraints from the fit to ND280 data.

The Bayesian analysis uses Markov Chain Monte Carlo (MCMC) to take random samples from the likelihood. The particular MCMC algorithm used is Metropolis–Hastings[57]. For a sufficiently large number of samples the Markov chain achieves an equilibrium probability distribution. The number of steps in the chain with a particular value of a parameter is proportional to the posterior probability that the parameter will have that value marginalized over all the other parameters. Credible intervals are then formed on the basis of highest posterior density, with bins of equal width in the parameter under study. Given the arbitrary initial state of the Markov chain, a finite number of samples must be obtained to allow the chain to converge to a state in which it is correctly sampling from the distribution. These preliminary 'burn-in' samples are discarded.

Data availability

The likelihood surface data that support these findings will be made available for public access on http://t2k-experiment.org/results/2020-constraint-cp-phase.

Code availability

The T2K collaboration develops and maintains the code used for the simulation of the experimental apparatus and statistical analysis of the raw data used in this result. This code is shared among the collaboration, but not publicly distributed. Inquiries regarding the algorithms and methods used in this result may be directed to the corresponding author.

34. Böhlen, T. et al. The FLUKA code: developments and challenges for high energy and medical applications. *Nucl. Data Sheets* **120**, 211–214 (2014).
35. Ferrari, A. Sala, P. R. Fasso, A. & Ranft, J. *FLUKA: A Multi-Particle Transport Code* Version 2005 CERN-2005–010, SLAC-R-773, INFN-TC-05–11 http://www.fluka.org/fluka.php?id=faq&sub=13 (FLUKA collaboration, 2005).
36. Brun, R. et al. *GEANT Detector Description and Simulation Tool* Report CERN-W5013 (CERN, 1994).
37. Abgrall, N. et al. Measurements of $\pi^{\pm}$, $K^{\pm}$, K^0_S, Λ and proton production in protoncarbon interactions at 31 GeV/c with the NA61/SHINE spectrometer at the CERN SPS. *Eur. Phys. J. C* **76**, 84 (2016).
38. Abe, K. et al. Measurements of the T2K neutrino beam properties using the INGRID on-axis near detector. *Nucl. Instrum. Methods A* **694**, 211–223 (2012).
39. Abgrall, N. et al. Measurements of $\pi^{\pm}$ differential yields from the surface of the T2K replica target for incoming 31 GeV/c protons with the NA61/SHINE spectrometer at the CERN SPS. *Eur. Phys. J. C* **76**, 617 (2016).
40. Abgrall, N. et al. Measurements of $\pi^{\pm}$, $K^{\pm}$ and proton double differential yields from the surface of the T2K replica target for incoming 31 GeV/c protons with the NA61/SHINE spectrometer at the CERN SPS. *Eur. Phys. J. C* **79**, 100 (2019).
41. Hayato, Y. A neutrino interaction simulation program library NEUT. *Acta Phys. Pol. B* **40**, 2477 (2009).
42. Llewellyn Smith, C. H. Neutrino reactions at accelerator energies. *Phys. Rep.* **3**, 261–379 (1972).
43. Nieves, J., Amaro, J. E. & Valverde, M. Inclusive quasielastic charged-current neutrino-nucleus reactions. *Phys. Rev. C* **70**, 055503 (2004).
44. Benhar, O. & Fabrocini, A. Two nucleon spectral function in infinite nuclear matter. *Phys. Rev. C* **62**, 034304 (2000).
45. Nieves, J., Simo, I. R. & Vacas, M. J. V. Inclusive charged-current neutrino-nucleus reactions. *Phys. Rev. C* **83**, 045501 (2011).
46. Gran, R., Nieves, J., Sanchez, F. & Vicente Vacas, M. J. Neutrino-nucleus quasi-elastic and 2p2h interactions up to 10 GeV. *Phys. Rev. D* **88**, 113007 (2013).
47. Rein, D. & Sehgal, L. M. Neutrino-excitation of baryon resonances and single pion production. *Ann. Phys.* **133**, 79–153 (1981).
48. Sjöstrand, T. High-energy physics event generation with PYTHIA 5.7 and JETSET 7.4. *Comput. Phys. Commun.* **82**, 74–89 (1994).
49. Oset, E., Salcedo, L. L. & Strottman, D. A theoretical approach to pion nuclear reactions in the resonance region. *Phys. Lett. B* **165**, 13–18 (1985).
50. Day, M. & McFarland, K. S. Differences in quasi-elastic cross sections of muon and electron neutrinos. *Phys. Rev. D* **86**, 053003 (2012).
51. Rein, D. Angular distribution in neutrino induced single pion production processes. *Z. Phys. C* **35**, 43–64 (1987).
52. Kabirnezhad, M. Single pion production in neutrino-nucleon interactions. *Phys. Rev. D* **97**, 013002 (2018).
53. Yang, T., Andreopoulos, C., Gallagher, H., Hoffmann, K. & Kehayias, P. A hadronization model for few-GeV neutrino interactions. *Eur. Phys. J. C* **63**, 1–10 (2009).
54. Jiang, M. et al. Atmospheric neutrino oscillation analysis with improved event reconstruction in Super-Kamiokande IV. *Prog. Theor. Exp. Phys.* **2019**, 053F01 (2019).
55. Wilks, S. S. The large-sample distribution of the likelihood ratio for testing composite hypotheses. *Ann. Math. Stat.* **9**, 60–62 (1938).
56. Feldman, G. J. & Cousins, R. D. A unified approach to the classical statistical analysis of small signals. *Phys. Rev. D* **57**, 3873–3889 (1998).
57. Hastings, W. K. Monte Carlo sampling methods using Markov chains and their applications. *Biometrika* **57**, 97–109 (1970).

Acknowledgements We thank the J-PARC staff for superb accelerator performance. We thank the CERN NA61/SHINE Collaboration for providing valuable particle production data. We acknowledge the support of MEXT, Japan; NSERC (grant number SAPPJ-2014-00031), the NRC and CFI, Canada; the CEA and CNRS/IN2P3, France; the DFG, Germany; the INFN, Italy; the National Science Centre and Ministry of Science and Higher Education, Poland; the RSF (grant number 19-12-00325) and the Ministry of Science and Higher Education, Russia; MINECO and ERDF funds, Spain; the SNSF and SERI, Switzerland; the STFC, UK; and the DOE, USA. We also thank CERN for the UA1/NOMAD magnet, DESY for the HERA-B magnet mover system, NII for SINET4, the WestGrid and SciNet consortia in Compute Canada, and GridPP in the United Kingdom. In addition, participation of individual researchers and institutions has been further supported by funds from the ERC (FP7), "la Caixa" Foundation (ID 100010434, fellowship code LCF/BQ/IN17/11620050), the European Union's Horizon 2020 Research and Innovation Programme under the Marie Sklodowska-Curie grant agreement numbers 713673 and 754496, and H2020 grant numbers RISE-RISE-GA822070-JENNIFER2 2020 and RISE-GA872549-SK2HK; the JSPS, Japan; the Royal Society, UK; French ANR grant number ANR-19-CE31-0001; and the DOE Early Career programme, USA.

Author contributions The operation, Monte Carlo simulation, and data analysis of the T2K Experiment are carried out by the T2K Collaboration with contributions from all collaborators listed as authors on this manuscript. The scientific results presented here have been presented to and discussed by the full collaboration, and all authors have approved the final version of the manuscript.

Competing interests The authors declare no competing interests.

Additional information

Correspondence and requests for materials should be addressed to M.H.

Peer review information *Nature* thanks Anatael Cabrera, Alexandre Sousa and the other, anonymous, reviewer(s) for their contribution to the peer review of this work.

Reprints and permissions information is available at http://www.nature.com/reprints.

Extended Data Table 1 | Systematic uncertainties

Type of Uncertainty	$\nu_e/\bar{\nu}_e$ Candidate Relative Uncertainty (%)
Super-K Detector Model	1.5
Pion Final State Interaction and Rescattering Model	1.6
Neutrino Production and Interaction Model Constrained by ND280 Data	2.7
Electron Neutrino and Antineutrino Interaction Model	3.0
Nucleon Removal Energy in Interaction Model	3.7
Modeling of Neutral Current Interactions with Single γ Production	1.5
Modeling of Other Neutral Current Interactions	0.2
Total Systematic Uncertainty	6.0

The systematic uncertainty on the predicted relative number of electron neutrino and electron antineutrino candidates in the SK samples with no decay electrons.